**Title:** What is that molecular machine really doing? Automated exploration of alternative transporter mechanisms

**Authors:** August George[1], Paola Bisignano[2], John Rosenberg[3], Michael Grabe[2], Daniel M Zuckerman[1*]

[*] zuckermd@ohsu.edu

**Affiliations:** [1]OHSU Center for Spatial Systems, Dept. of Biomedical Engineering, OHSU. [2]Cardiovascular Research Inst., UCSF. [3]Dept. of Biological Sciences, Univ. Pittsburgh.

**Keywords:** computational biology, chemical physics, molecular machines, kinetic models, biochemical networks, Monte Carlo, cotransporters, symporters, antiporters, computational methods, Markov models

**Abstract:** Do complex molecular machines tend to exhibit a single mechanism, as suggested in literature and textbook cartoons, or is a multiplicity of pathways possible or even prevalent? Motivated by growing evidence for pathway heterogeneity, we develop theoretical and computational approaches for investigating this question, which could have significant potential impact in both understanding molecular-scale cell biology and in the design of synthetic machines. Focusing on transport in this initial study, we pursue Monte Carlo exploration of "model space." Trial moves adjust transition rates among an automatically generated set of conformational and binding states while maintaining fidelity to thermodynamic principles and fitness goal. The simulations yield both single-mechanism and heterogeneous multi-mechanism models for cotransport in a simple environment. In a "competitive" environment with a decoy substrate, several qualitatively distinct models are found which are capable of extremely high discrimination coupled to a leak of the driving ion. The array of functional models would be difficult to find by intuition alone in the complex state-spaces of interest.

**Introduction:**

The proteins and protein complexes known as molecular machines perform essential functions in the cell, such as transport, locomotion, energy production, and gene expression [1]. Of special interest in this initial study are the transport proteins that move ions and small molecules across a membrane [1] using an electrochemical gradient [1], such as the SGLT family of transporters. SGLT transporters are of biomedical interest due to the vital role that SGLT1 and SGLT2 play in the uptake of glucose in the small intestines and kidney [2]. As SGLT2 inhibitors have continued to develop, there has been renewed interest in the mechanisms, kinetics, and functions of glucose transport proteins [3] [4] [5] [6].

The biological mechanisms of transporters as well as other molecular machines can be modeled using biochemical networks, typically along with mass action kinetics [7]. In a biochemical network, the system is decomposed into discrete states connected by transition rates between states [7] forming a network of interconnected reactions in the state-space. These networks can be modeled using the chemical master equation: a set of differential equations describing the state probabilities and connected transition rates for each state [8]. Biochemical networks are generally Markovian [9], have a number of different control patterns [10], and adhere to specific design principles [11].

One of the most remarkable properties of some molecular machines is the ability to perform "proofreading" or error-correction [12] [13] [14]. Specifically, certain network topologies promote

enhanced selectivity (i.e. reduced error) in systems with a competing substrate [12] [13] [14], a phenomenon known as proofreading; this enhancement in selectivity incurs a free energy cost, typically paid via hydrolysis of a phosphate bond. While aspects of proofreading such the speed/accuracy tradeoff [15], the log-response of proofreading [16], and its non-equilibrium applications [17] have been examined, there has been little mention of transporters [18] [19], exhibiting a similar behavior in the literature.

Despite the complex state-spaces accessible to molecular machines such as transporters, their mechanisms are often described using a single-pathway, highly machine-like cartoon-like model [1] [20] [21]. While such models are helpful for a qualitative understanding of complex protein behavior and chemical networks, they may also build in unwarranted assumptions about the system. There is growing evidence that molecular machines may exhibit complexity beyond that embodied in typical textbook cartoons [22] [23]. Recent experimental studies have shown that certain traditional model assumptions such as fixed stoichiometry [24] [25], homogenous pathways [26], and constrained binding sites [27] may be incorrect.

Due to the challenges (such as large state-spaces) of modelling complex biochemical networks of interest, new approaches have been developed to computationally model these systems. Genetic-algorithm sampling methods have been used [28] [29] to evolve complex biochemical networks such as metabolic pathways [30]. In addition, a computationally efficient matrix method has been developed for use on ion channel network models [31]. While these methods have shown promising results, they do not impose thermodynamic consistency (cycle constraints based on detailed balance) which is a necessary condition for physical systems [7].

Motivated by the possibility of discovering new potential mechanisms and the limitations of current approaches, we have developed a new approach that systematically explores the biochemical network model space for a given molecular machine. Our approach generates diverse models that are both thermodynamically consistent and testable. Due to their biomedical significance, we first examined transporters motivated by SGLT type proteins. Our results suggest there is a diverse set of possible mechanisms for these cotransporters, including Hopfield-like kinetic proofreading.

**Methods:**

We have developed custom software, ModelExplorer, to model molecular machine behavior. Although this study is focused primarily on membrane co-transporters, the software is designed to be general enough for the exploration of other molecular systems. ModelExplorer automatically generates combinatorial state spaces and then uses a modified Monte Carlo Metropolis algorithm to sample the (Markov) model space with a user-defined “energy” or fitness function. This fitness function could embody experimental measurements via a weighted sum of residuals, but here we use functionality-inspired fitness functions.

We create a system model consisting of states and connecting rate constants, with energies assigned to each state and state transition. Systems states are created from all the allowed combinations of string subunits, and placed into physically equivalent groupings. The Monte Carlo sampling will generate a “fitness trajectory” in model space that allows the selection of the fittest models, with a tempering procedure used to avoid trapping. Selected models may then be analyzed for kinetic pathways as well as

flow stoichiometry over a range of chemical potential conditions, resulting in experimentally testable models.

Models generated with ModelExplorer are assessed based on their non-equilibrium steady-state behavior, and are constructed to be consistent with thermodynamic principles. At steady-state conditions, the thermodynamic states (e.g. concentration) of a system held are constant in time [8]. The behavior of our non-equilibrium models is determined by the rate constants governing transitions among the states. To ensure thermodynamic consistency among all rate constants [7] we use an energy-based formulation where each state and transition are given an energy, and the rate is expressed as:

$$k_{ij} = e^{\Delta\Delta\mu_{ij}} k_0 e^{-(E_{bar} - E_i)}$$

where $\Delta\Delta\mu_{ij}$ corresponds to the difference in the log of concentration difference of state 'i' vs. equilibrium and the log of concentration difference of state 'j' vs. equilibrium. These non-equilibrium energy terms are calculated for each state with user defined parameters (e.g. fraction of $d\mu_i$ attributed to outside the cell). $K_0$ is the user-defined prefactor. $E_{bar}$ corresponds to the transition state energy for state 'i' to state 'j' and $E_i$ corresponds to the energy of state 'i'. All energies are effectively in $k_BT$ units. Our rate formulation is equivalent to the ligand concentration multiplied by the Arrhenius equation [32]:

$$k = k_0 e^{\frac{-E_a}{K_b T}}.$$

We use strings of characters to construct the state space for a molecular machine. This is best illustrated with an example for a hypothetical alternating-access transporter of substrate (S) driven by a sodium ion (N): the state "OF-Nb-Si" represents the outward-facing (OF) conformation with a sodium bound (Nb) and substrate inside the pertinent cell or organelle. The string OF-Nb-Si fully defines the system state in a sufficient way for our kinetic scheme explained below. The state string consists of a set of 'base state' strings, each of which describes a different characteristic of the machine. For a transporter, this includes the conformational state (inward or outward facing; IF or OF), sodium-ion state (bound to protein, intracellular/"inside", or extracellular/"outside"; Nb, Ni, or No), and a substrate binding state (Sb, Si, or So), resulting in a 3D state space. To examine transport mechanisms in heterogeneous environments we add an additional binding base state for the competing substrate (W) following the same conventions (Wb, Wi, or Wo), resulting in a 4D state space. The set of states result from combinatorial joining of base-state strings, filtering out any user-defined exclusions such as mutually exclusive substrate binding, to create the final high-dimensional state space. This state-space is then mapped to a lower-dimensional space of conformationally unique states, allowing for more efficient state population calculations.

We use the Monte Carlo (MC) Metropolis algorithm [33] [34] with tempering to sample our model space, where a trial move consists of randomly adjusting a state or transition, and its equivalent "tied" members. Here, "tied" members are considered any state (or transition) which is physically equivalent given a steady state where the outside and inside concentrations are fixed. For example, OF-Nb-Si and OF-Nb-So are physically equivalent states because concentrations of the **S**ubstrate "**i**nside" and "**o**utside" of the cell are constant. Adjusting all the "tied" states during a trial move prevents physically

equivalent states in the model from having non-equivalent energies, maintaining thermodynamic consistency. We then construct a rate matrix for the new model using the equilibrium and non-equilibrium (binding) energies for each state/transition along with the modified Arrhenius equation (shown above). Solving this updated matrix yields the steady state probabilities for each state/transition, from which we can calculate the flows between states [35]. Each model will be have a Monte Carlo 'energy' assigned (i.e. fitness score) based on a user-defined general function (i.e. substrate flow into the cell). By convention, lower fitness scores are more fit. The current model 'energy' will be compared the previous model's energy and accepted/rejected based on the Metropolis criterion [33] [34]:

$$\text{If } \Delta E \leq 0\text{: Accept new model}$$

$$\text{Else: Accept new model with transition probability, } p = e^{-\beta \Delta E}$$

Where ΔE corresponds to the change in the Monte Carlo 'energies' of the two models, and β is the inverse 'temperature' parameter.

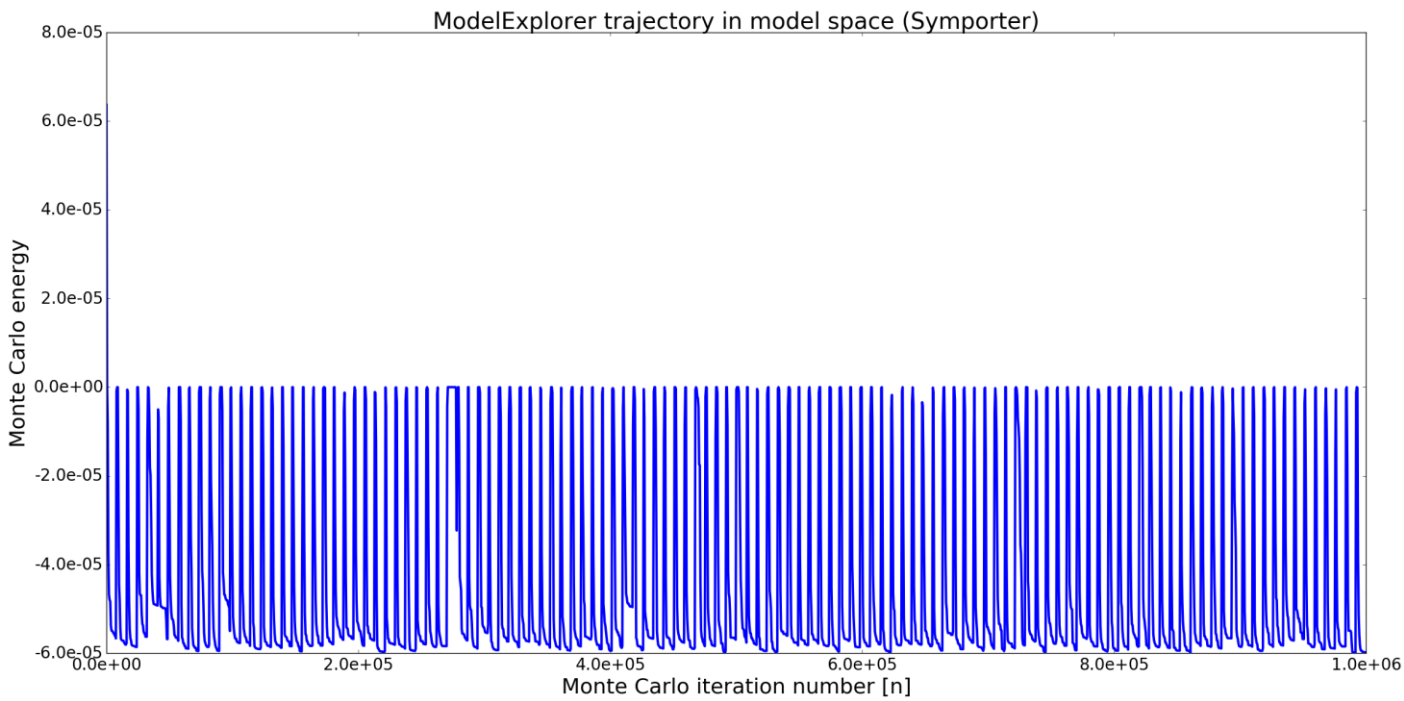


**Figure 1:** Exploration of model space using Markov-chain Monte Carlo. The plot shows a ModelExplorer trajectory based on symporter energy function (no decoy) during a 1e6 MC step simulation. Note that *each point represents a different kinetic model*. Energy minima correspond to more fit models using $E_{MC}$ = - $flow_{Substrate}$ as a fitness function. Models are initially at a high energy but quickly find local minima. A tempering schedule of alternating temperature increases and decreases prevents the simulation from being trapped in local minima.

Since each Monte Carlo step results in a model (set of rate constants and connecting states), the simulations will result in a Monte Carlo trajectory in model space – i.e., a sequence of models. In order to avoid being trapped in deep "energy" (high fitness) basins we employ a tempering [36] procedure.

This procedure adjusts the beta parameter in the Metropolis acceptance criterion, facilitating exploration different areas in the model space because of the increased likelihood of acceptance. ModelExplorer allows for both automated and manual tempering. Automated tempering tracks the change in fitness of the previous models, decreasing beta (heating) if the fitness has not changed over several models, and then increasing beta (cooling) once a user-defined threshold is met. Manual tempering sets a fixed heating and cooling schedule for the duration of the simulation. The tempering procedure is fully customizable and increases the diversity of models found in a simulation. **[Figure 1]** is an example of the Monte Carlo "energy" trajectory in model space produced in ModelExplorer for a simple symporter system. Note that the initial models are not fit (positive MC energy), but eventually fit models are found.

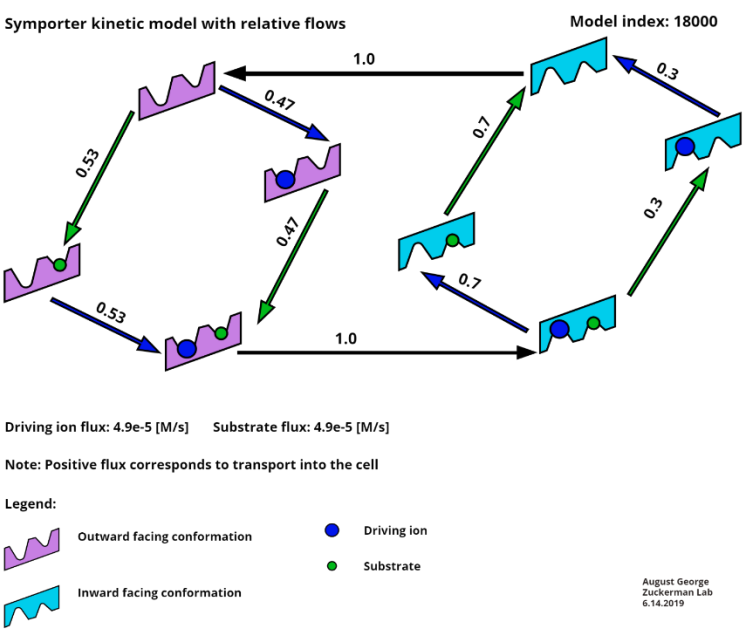


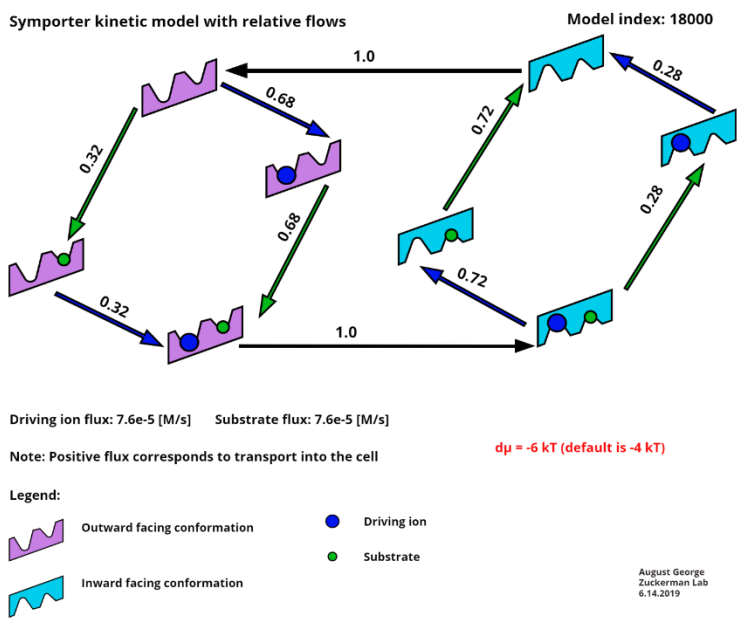


**Figure 2a (left):** Example symporter model. Relative flows, normalized by the maximum flow, are shown for a particular symporter model (index 18000) found during the 1e6 MC step symporter simulation. This model employs a combination of two simple pathways, thus differing from traditional symporter cartoons, while still maintaining a 1:1 ratio of ion to substrate flux. Note that the absolute flux values are not physically relevant due to arbitrary overall constant prefactor (i.e. all flows can be scaled by an arbitrary constant and remain consonant with the governing equations). **Figure 2b (right):** The same model can be analyzed at different fixed ion chemical potential differences (essentially concentrations). A kinetic pathway model (index 18000) for a symporter found during the 1e6 MC step symporter simulation with the ion chemical potential difference = -6 $k_BT$ instead of the default -4 $k_BT$. Note that the network topology is the same, with different relative flows, and different substrate and ion fluxes.

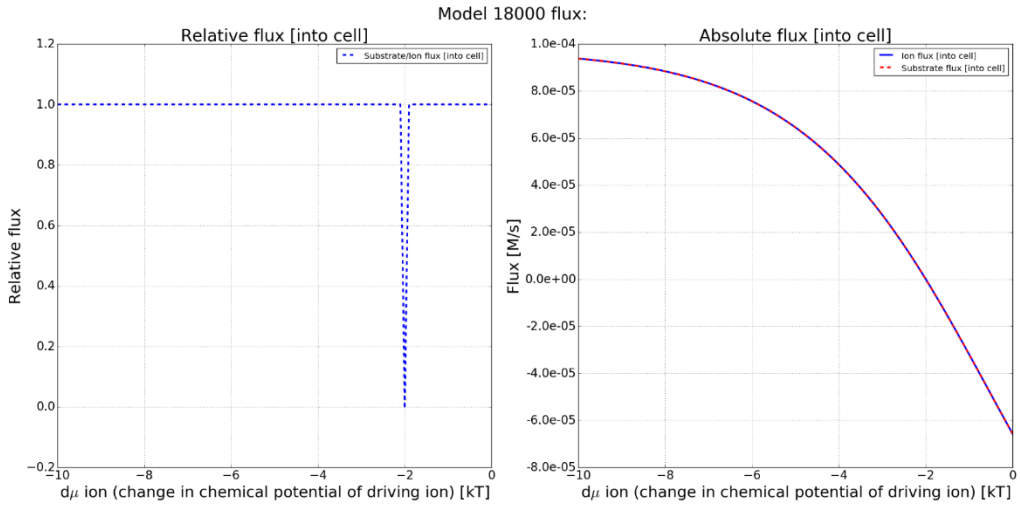


**Figure 2c:** The relative and absolute flux of the driving ion and substrate of the same model (index 18000) are shown. This allows the analysis of stoichiometry and flux information for the given model. The fluxes from the kinetic pathways directly correspond to the fluxes shown in the absolute flux graph. Note the 1:1 stoichiometry of the substrate to ion flux, indicating an ideal symporter with no leaks. At the ion chemical potential difference = -2 $k_BT$, the substrate chemical potential difference is equal and opposite, resulting in no flux.

Selected models can be analyzed in several ways using ModelExplorer: by characterizing overall stoichiometries, kinetic pathway analysis, and manual adjustment of selected transition rates. The flows of a model can be calculated over a range of chemical potential by incrementing the desired chemical potential and updating the non-equilibrium energy terms for each state. The rates, steady state probabilities, and flows are then recalculated for each chemical potential increment, allowing for the examination of flow stoichiometry. ModelExplorer also calculates the net flux between states, which is used to create a kinetic pathway diagram for a specific model and chemical potential difference. Furthermore, individual models may be perturbed by modifying specific state/transition energies, leading to insights on pathway characteristics (e.g. pathway with or without leaks). Combining the kinetic pathway diagram with the flow analysis provides an insightful method to investigate the dynamic behavior of molecular machines and provide testable mechanistic models **[figure 2]**.

In addition to single model analysis, we have developed tools for the meta-analysis of simulations. A simple data pipeline allows for the analysis of sampling parameters, run-to-run model distributions, and model clustering, based on the differences in model flows. Sampling efficiency can be evaluated based on the average time to find a sufficiently different model (i.e. cluster) during the simulation as well as the run-to-run comparison. The run-to-run comparison tool computes the minimum distance between models found in simulation 'A' compared to simulation 'B' and vice versa, generating a model distribution between the runs. This provides insight into possibly unique models found under different simulation conditions. Models may also be clustered hierarchically [37], allowing for the discovery of different model classes. The model differences are calculated using the Euclidean distance between the vectors of normalized net flows between states for a given model.

ModelExplorer has a number of adjustable physical parameters (dμ - change in chemical potential), simulation parameters (seed, run length), sampling parameters (tempering schedule, amount to perturb a state/barrier energy, as well as constraints (illegal transitions and states) for a simple cotransport

system. In order to investigate Hopfield-like enhanced discrimination [12], the cotransport system with a decoy substrate has additional parameters and constraints. The decoy-bound state energies differ from their equivalent substrate-bound states by a fixed amount (ΔΔG parameter), and have equal barrier energies. This constraint forces the enhanced selectivity to result from the difference in binding affinities alone, and not "internal proofreading", which is consistent with Hopfield's kinetic proofreading network [12]. Furthermore, for simplicity, occluded states and mutual binding states of the substrate and decoy have been disabled.

**Results:**

We present results for a simple symporter (cotransporter) system and for a transporter 'challenged' by a decoy substrate. For a simple cotransporter system without a decoy, the results include validation of ideal symporter/antiporter mechanisms, selected network topologies, and substrate/ion flux for a range of ion chemical potential differences. For cotransporters with an additional decoy substrate, we analyze several features of four simulations: selected network topologies, substrate/decoy/ion flux for varying ion chemical potential differences, network heterogeneity via clustering, and possible alternative mechanisms.

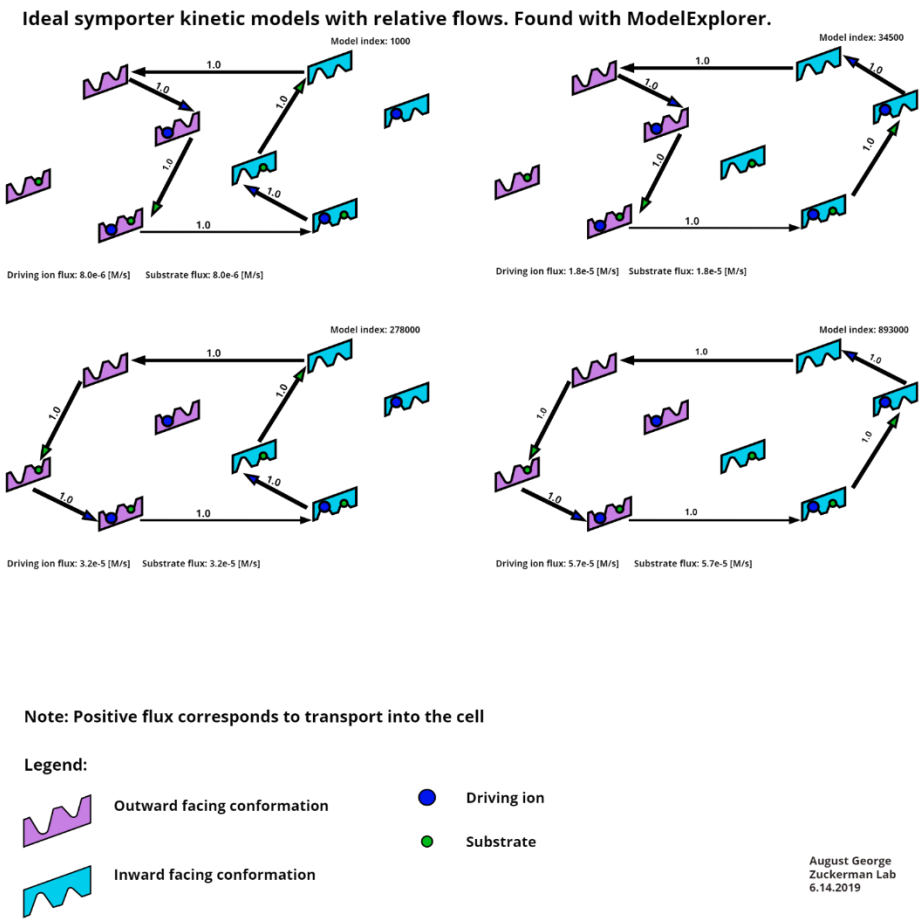

**Figure 3:** Finding multiple pathways. All four ideal symporter pathways are generated during a 1e6 MC step ModelExplorer simulation using a fitness function (Monte Carlo energy) $E_{MC,Symport}$ = - $flow_{Substrate}$. These ideal pathways correspond to the lowest number of connected states that still achieve the functional goal of symporting. Note that the absolute flux values are not physically relevant due to arbitrary overall constant prefactor (i.e. all flows can be scaled by an arbitrary constant and remain consonant with the governing equations).

We first studied a transporter system with a single substrate driven by an ion gradient. To explore the symporter behavior of this model, the substrate chemical potential difference was set to 2 $k_BT$ and the ion chemical potential difference set to -4 $k_BT$. The fitness goal (Monte Carlo energy) was set to:

$$E_{MC,Symport} = -flow_{Substrate,}$$

promoting intracellular substrate flow along the ion gradient. The simulation of 1e6 MC steps yielded the four idealized symporter cycles, as well as combinations of the idealized symporter cycles. All of these models consist of a 1:1 ratio of substrate and ion flux into the cell - consistent with the theoretical predications of an optimized symporter **[figure 3]**.

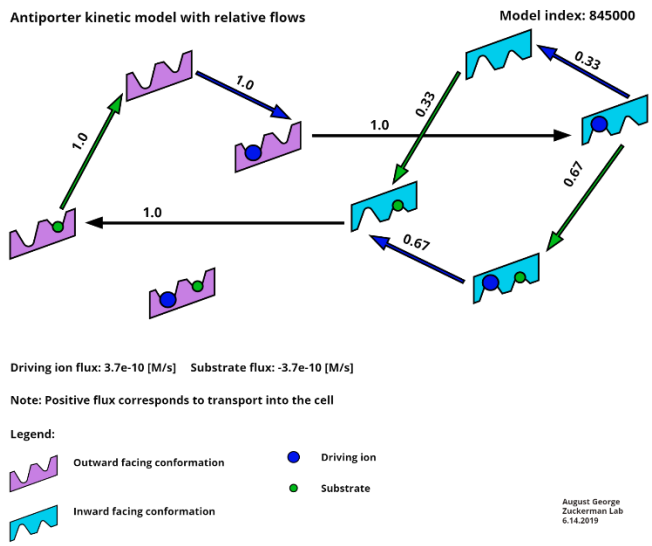


**Figure 4a:** Selected antiporter pathway model (index 845000) from 1e6 MC step simulation. This model shows a combination of pathways, which differ from the traditional antiporter representation while still maintaining a 1:1 ratio of ion to substrate flux. Note that the absolute flux values are not physically relevant due to arbitrary overall constant prefactor (i.e. all flows can be scaled by an arbitrary constant and remain consonant with the governing equations).

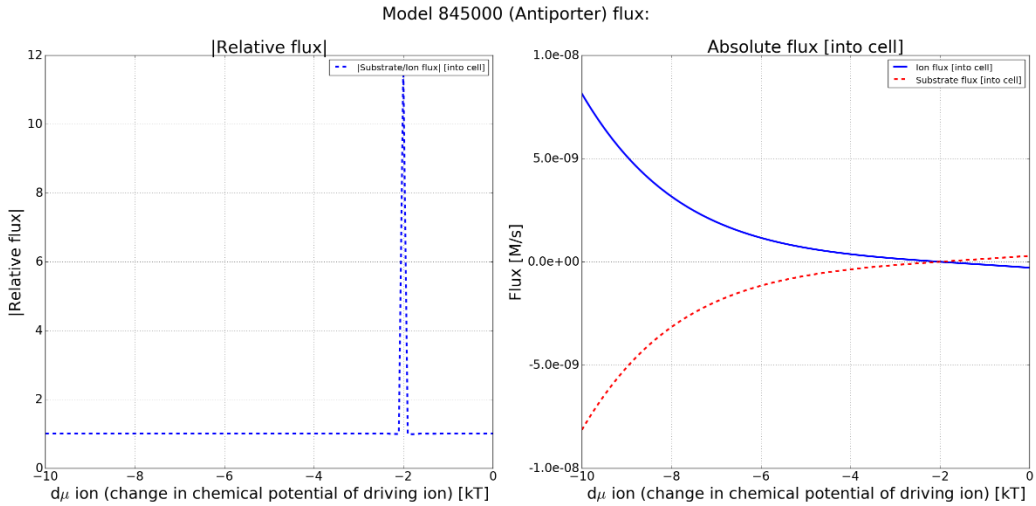


**Figure 4b:** The relative and absolute flux of the driving ion and substrate of the same antiporter model (index 845000) are shown. *For the relative flux, the absolute value is taken to show the substrate to ion stoichiometry.* The fluxes from the kinetic pathway directly corresponds to the flux shown in the absolute flux graph. Note the 1:1 stoichiometry of the substrate to ion flux, indicating an ideal antiporter with no leaks. At the ion chemical potential difference = -2 $k_BT$, the substrate chemical potential difference has the same magnitude; the flux of the ion approaches zero resulting in an increase of the relative flux of substrate to ion.

Antiporter behavior of the same state space was tested by modifying the substrate chemical potential difference to -2 $k_BT$ and setting the fitness goal to:

$$E_{MC,Antiport} = +flow_{Substrate}$$

promoting extracellular flow of the substrate against the ion gradient**.** The simulation of MC n = 1e6 steps yielded antiporter models consisting of a 1:1 ratio of substrate flux out of the cell and ion flux into the cell - consistent with the theoretical predications of an optimized antiporter **[figure 4].**

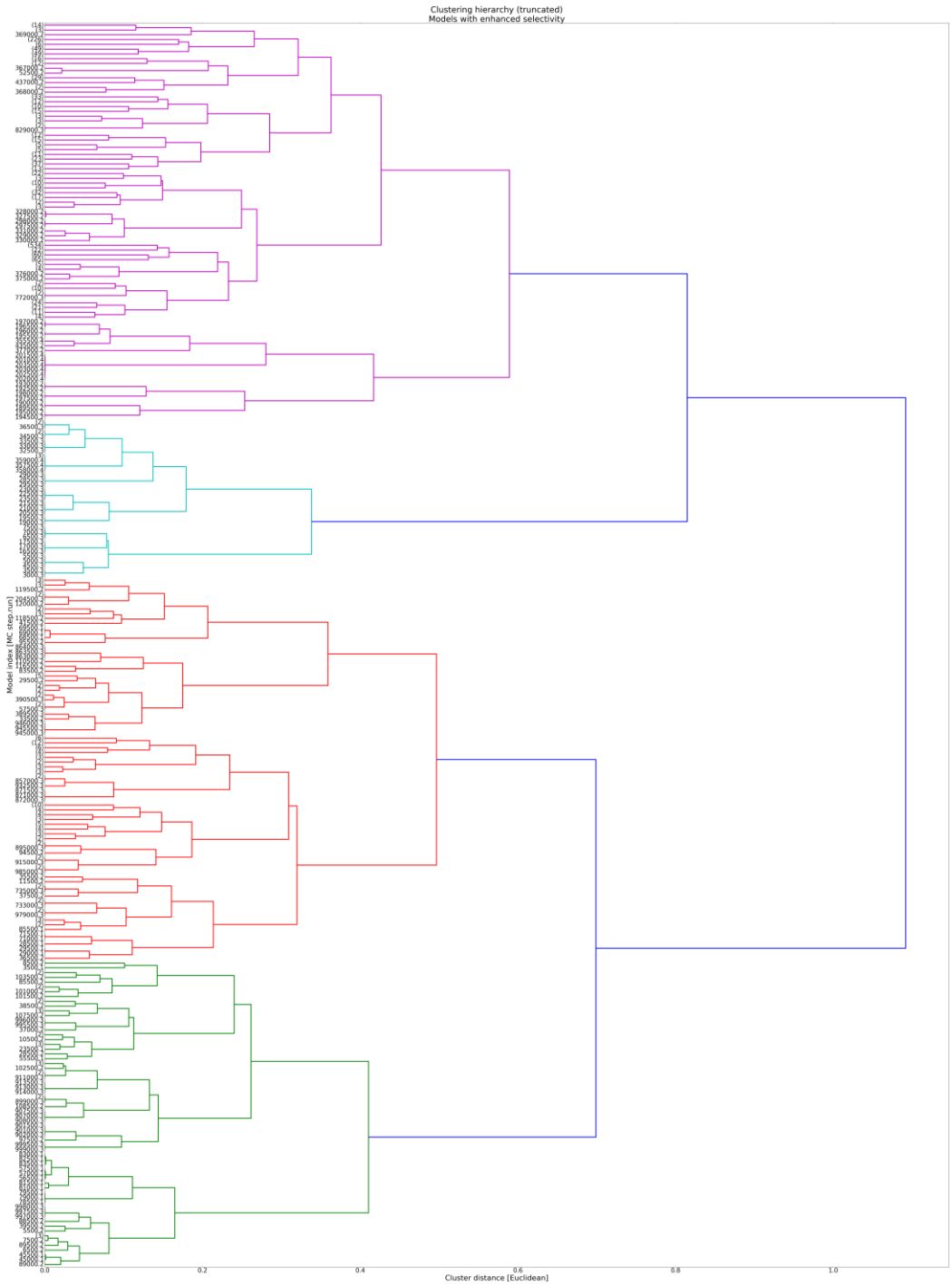


**Figure 5:** Discovery of highly diverse models. The plot shows hierarchical clustering (truncated) of cotransport models with enhanced selectivity of a substrate over a decoy substrate. 8000 models were aggregated from four separate runs with different sampling parameters. The models were filtered for enhanced selectivity, defined as models where the sodium ion to substrate flux ratio is greater than 0.1, and the substrate to decoy flux ratio being greater than $10e^1$ ($\Delta\Delta G = 1\ k_BT$).The models were clustered based on a Euclidean distance metric of the flows of each model using the complete-linkage strategy. The distance threshold of 0.65 is empirically found to lead to distinct mechanism classes with qualitatively different pathways. The dendrogram was truncated to eight levels for visual clarity. The number of nodes below the truncated node are shown in parenthesis.

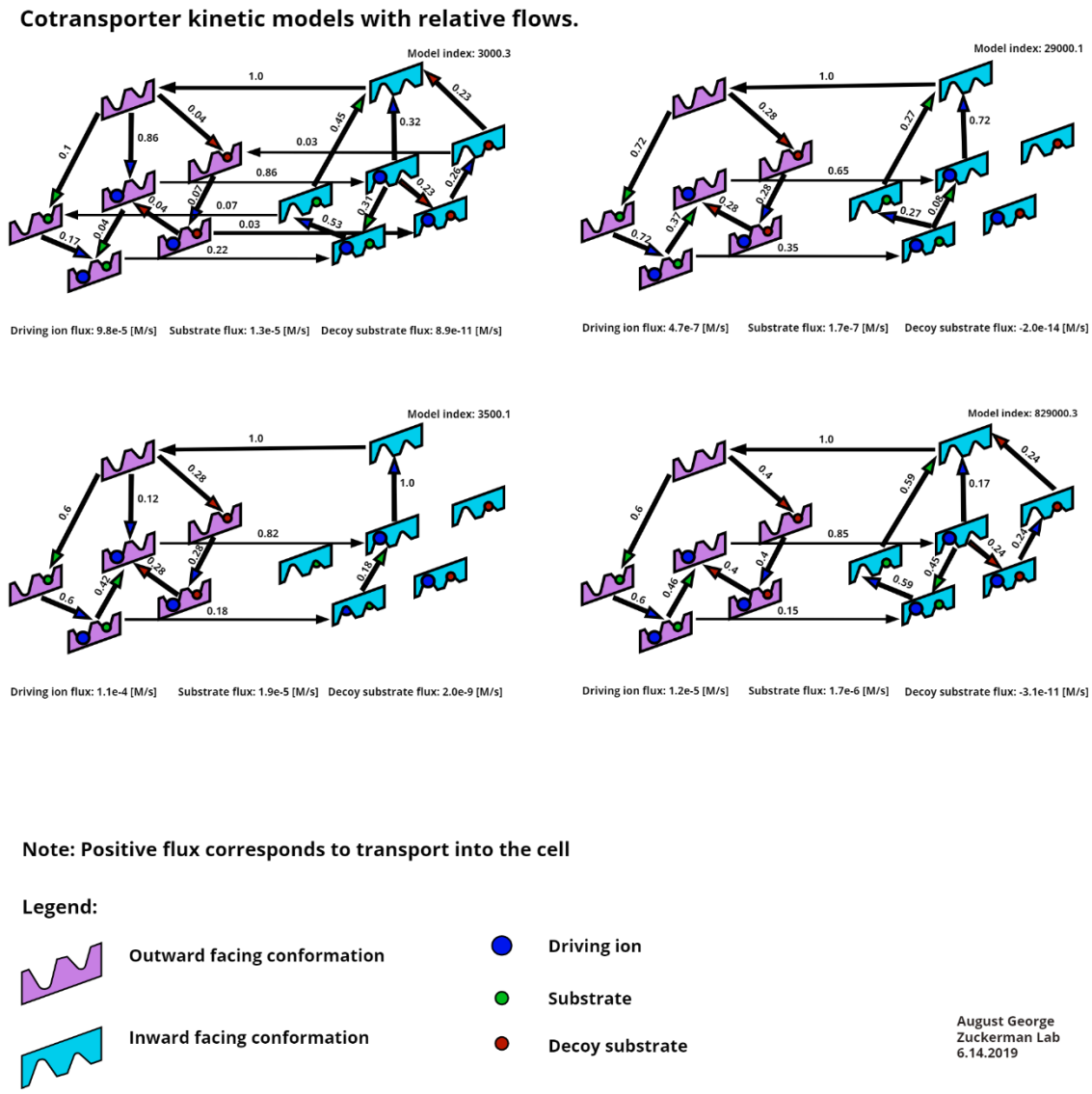


**Figure 6:** Collection of enhanced selectivity model classes from four combined simulations. The hierarchal clustering with complete-linkage found four clusters at a Euclidean distance threshold of 0.65. Below are representative models for each cluster, which exhibit a high level of selectivity and a fair amount of model diversity. Note that the absolute flux values are not physically relevant due to arbitrary overall constant prefactor (i.e. all flows can be scaled by an arbitrary constant and remain consonant with the governing equations).

To investigate whether symporter models are capable of enhancing selectivity beyond that generated by their differing affinities [$\Delta\Delta G = 1\ k_BT$], a competing decoy substrate was added to a transport system with a substrate driven by an ion gradient. The substrate chemical potential difference and decoy chemical potential difference were set to 2 $k_BT$, and the ion chemical potential difference was set to -4 $k_BT$. The fitness goal (Monte Carlo energy) was set to:

$$E_{MC} = -flow_{substrate}\left(\frac{|flow_{substrate}+\varepsilon|}{|flow_{decoy}+\varepsilon|}\right)^{\alpha}$$

where α allows for weighting of the substrate to decoy flow ratio, and ε = 1e-15 improves numerical stability. To reduce runtime and memory requirements, models were stored every 500 MC steps. Four separate simulation of 1e6 MC steps with α = 1 were conducted at different sampling conditions with each simulation outputting 2000 models. The models from each run were combined and then filtered based on the sodium ion to substrate ratio being greater than 0.1, and the substrate to decoy ratio being greater than $10e^{\Delta\Delta G}$, where ΔΔG = 1 [38]. This resulted in 1783 (22%) of the aggregate 8000 models exhibiting enhanced selectivity. These models were then clustered based on the flows between states using a Euclidean distance metric with complete-linkage. Based on a distance threshold of 0.65, found through trial and error, there were four different model classes with differing kinetic pathways **[figures 5-6]**.

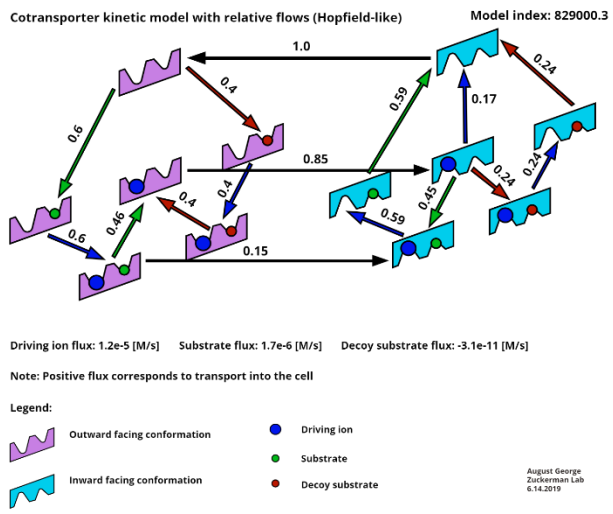


**Figure 7a:** Hopfield-like "proofreading" model (index 829000.3) from a 1e6 MC step simulation. The majority of the models with enhanced selectivity (as defined earlier) have a network that resembles the Hopfield kinetic proofreading network (purple cluster in dendrogram). This network model has an extra unbinding step for both the substrate and decoy substrate. Due to the differences in binding affinities (ΔΔG = 1 $k_BT$) the substrate is favored to re-enter the reaction network compared to the decoy substrate. Over a narrow range of concentrations, this model has an unbounded discrimination (substrate to decoy) ratio as the decoy flux approaches zero. Note that the absolute flux values are not physically relevant due to arbitrary overall constant prefactor (i.e. all flows can be scaled by an arbitrary constant and remain consonant with the governing equations).

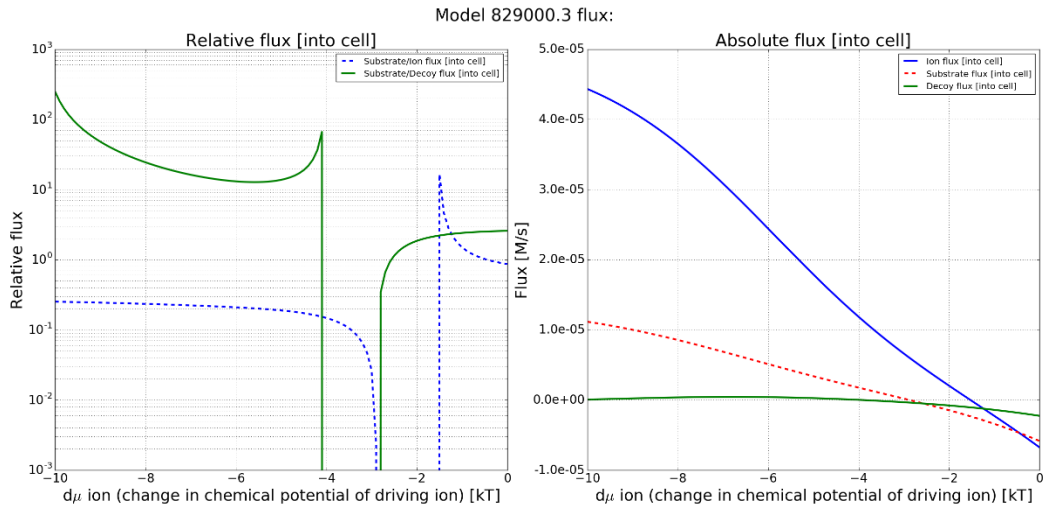


**Figure 7b:** Flux diagram of the Hopfield-like proofreading model. Note that while the model is optimized at ion chemical potential difference = -4 $k_BT$, there is also enhanced discrimination at larger ion chemical potential difference (concentration) values. Also, note that there is a regime with low ion chemical potential difference where the substrate and the decoy have negative flux (i.e. leak outside of the cell).

The most populated class had a kinetic pathway similar to the Hopfield proofreading models **[figure 7]** that had an extra unbinding step for both the substrate and the decoy in the outward facing conformation, as well as symmetry in the inward and outward facing conformations. The model classes also contain non-intuitive pathways **[figure 8]**, highlighting moderate model diversity based on the preliminary data.

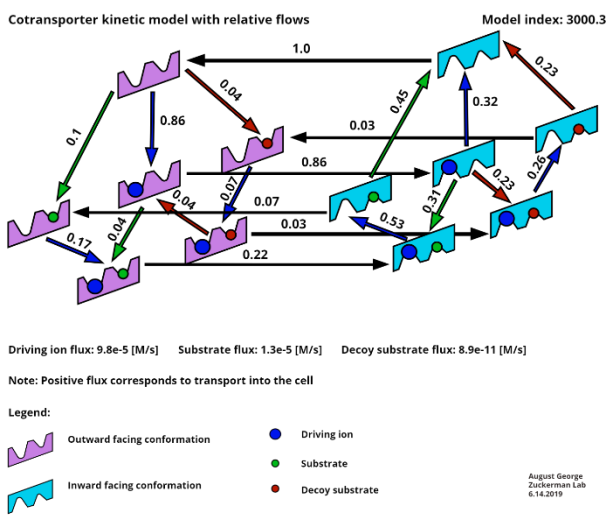


**Figure 8a:** Kinetic pathway of a selected model (index 3000.3) with enhanced selectivity. Note that the states in this model are full connected, forming a complex network structure that is a non-intuitive. Over a narrow range of concentrations, this model has an unbounded discrimination (substrate to decoy) ratio as the decoy flux approaches zero. Note that the absolute flux values are not physically relevant due to arbitrary overall constant prefactor (i.e. all flows can be scaled by an arbitrary constant and remain consonant with the governing equations).

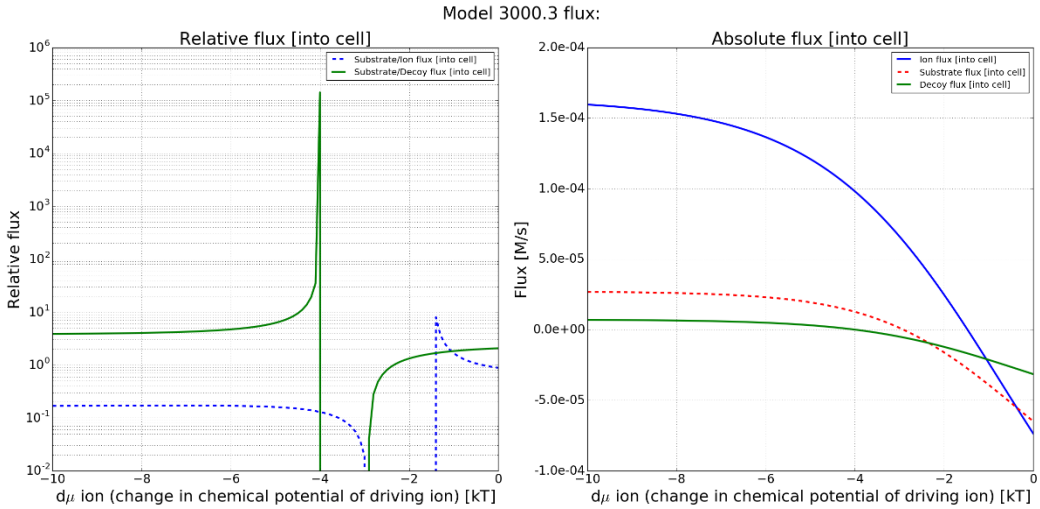


**Figure 8b:** Flux diagram of the same model (index 3000.3) with enhanced selectivity. Note that the model is optimized at ion chemical potential difference = -4 $k_BT$ Also, note that there is a regime with low ion chemical potential difference where the substrate and the decoy have negative flux (i.e. leak outside of the cell).

**Discussion:**

The results indicate that our method can find diverse, testable models that provide insight into more complicated cotransport systems. The model-sampling approach systematically found kinetic pathways for both simple symporters and antiporters, including mixed ideal pathways, validating our approach as applied to simple transport systems. The preliminary data also indicates the possibility of cotransporters that exhibit enhanced selectivity similar to Hopfield's kinetic proofreading models. This suggests an apparently new potential alternative mechanism for secondary active transporters. The results from clustering show a fairly diverse group of model classes that exhibit enhanced selectivity using different kinetic pathways.

While the data gives us a better understanding of our method's capabilities, there are several areas of improvement for future work. Sampling models in the 'competitive' transporter state-space has proven to be challenging and will require further optimization. Furthermore, new functionality will need to be added to ensure sufficient sampling, such as initializing several separate simulations using a Latin hypercube [39]. Once the sampling issues have been resolved, we plan to provide tighter integration with experimental data, with a future goal of generating kinetic models based on the data, as well as adapting our method to model experimental data by changing the fitness function. Finally, we plan to apply our method to model complex molecular machines such as the ATP synthase.

**Conclusions**

In light of new evidence for the alternative behavior of molecular machines, we have developed a thermodynamically consistent approach to systematically explore their state-space, generating experimentally testable kinetic models based on a predetermined fitness function. Our method was first applied to a cotransporter system with and without a decoy substrate. Preliminary results have validated our method against 'textbook' symporter/antiporter models, and have generated a variety of mechanisms that enhance selectivity – including a Hopfield-like proofreading network, which could have important future biomedical applications.

**Acknowledgements:** Barmak Mostofian, and Jeremy Copperman for helpful discussions. Research supported by NSF Grant MCB-1715823.

**References:**

[1] B. Alberts, A. Johnson, J. Lewis, M. Raff, K. Roberts and a. P. Walter, Molecular Biology of the Cell, New York: Garland Science, 2002.

[2] S. B. Poulsen, R. A. Fenton and T. Rieg, "Sodium-glucose cotransport," *Current Opinion in Nephrology and Hypertension,* vol. 24, no. 5, pp. 463-469, 2015.

[3] D. Oleg, Y. Tatiana, K. Dmitry and D. Oleg, "Analysis of the efficacy of SGLT2 inhibitors using semi-mechanistic model," *Frontiers in Pharmacology,* vol. 5, p. 218, 2014.

[4] D. Deng and N. and Yan, "GLUT, SGLT, and SWEET: Structural and mechanistic investigations of the glucose transporters.," *Protein Science,* vol. 25, pp. 546-558, 2016.

[5] P. Bisignano, C. Kalyanaraman, C. Ghezzi, E. M. Wright, J. Abramson, A. Paz, M. P. Jacobson, R. Friemann and M. Grabe, "Structural Insights into Sodium-Dependent Sugar Transporters and their Inhibition Mechanism,," *Biophysical Journal,* vol. 112, no. 3, p. 128a, 2017.

[6] E. M. Wright, C. Ghezzi and D. D. F. and Loo, "Novel and Unexpected Functions of SGLTs," *Physiology,* vol. 32, no. 6, pp. 435-443, 2017.

[7] T. L. Hill, Free Energy Transduction and Biochemical Cycle Kinetics, Springer, 1989.

[8] D. Schnoerr, G. Sanguinetti and a. R. Grima, "Approximation and inference methods for stochastic biochemical kinetics—a tutorial review," *Journal of Physics A: Mathematical and Theoretical,* vol. 50, no. 9, 2017.

[9] G.Jenkinson and J.Goutsias, "Markovian dynamics on complex reaction networks," *Physics Reports,* vol. 529, no. 2, pp. 199-264, 2013.

[10] V. Galstyan, L. Funk, T. Einav and a. R. Phillips, "Combinatorial Control through Allostery," *The Journal of Physical Chemistry B,* vol. 123, no. 13, pp. 2792-2800, 2019.

[11] W. Lim, C. Lee and Chao Tang, "Design Principles of Regulatory Networks: Searching for the Molecular Algorithms of the Cell," *Molecular Cell,* vol. 49, no. 2, pp. 202-212, 2013.

[12] J. J. Hopfield, "Kinetic Proofreading: A New Mechanism for Reducing Errors in Biosynthetic Processes Requiring High Specificity," *PNAS,* vol. 71, no. 10, pp. 4135-4139, 1974.

[13] J. Ninio, "Kinetic amplification of enzyme discrimination," *Biochimie,* vol. 57, no. 5, pp. 587-595, 1975.

[14] A. Fersht, "Editing mechanisms in protein synthesis. Rejection of valine by the isoleucyl-tRNA synthetase," *Biochemistry,* 1977.

[15] K. Banerjee, A. B. Kolomeisky and O. A. Igoshin, "Trade-off in biological error correction," *PNAS,* vol. 114, no. 20, pp. 5183-5188, 2017.

[16] M. Hemery and P. François, "In Silico Evolution of Biochemical Log-Response," *The Journal of Physical Chemistry B,* vol. 123, no. 10, pp. 2235-2243, 2019.

[17] A. Murugan, D. A. Huse and S. and Leibler, "Discriminatory Proofreading Regimes in Nonequilibrium Systems," *Phys. Rev. X,* vol. 4, no. 2, p. 021016, 2014.

[18] W. D. Stein and B. Honig, "Models for the active transport of cations - The steady-state analysis," *Molecular and Cellular Biochemistry,* vol. 15, no. 1, pp. 27-44, 1977.

[19] T. Chou, K. Mallick and a. R. K. P. Zia, "Non-equilibrium statistical mechanics: from a paradigmatic model to biological transport," *Reports on Progress in Physics,* vol. 74, no. 11, 2011.

[20] I. Sobczak and J. S. Lolkema, "The 2-Hydroxycarboxylate Transporter Family: Physiology, Structure, and Mechanism," *Microbiology and Molecular Biology Reviews,* vol. 69, no. 4, pp. 665-695, 2005.

[21] R. Schröder, S. F. Wulf, V. Ropars, S. Fujita-Becker, M. Oster, G. Hofhaus, L. G. Trabuco, O. Pylypenko, H. Lee Sweeney and A. Houdusse, "The Force Producing ADP State of Myosin Bound to Actin.," *PNAS,* vol. 110, no. 3, p. 13a, 2016.

[22] K. E. Mangold, B. D. Brumback, P. Angsutararux, T. L. Voelker, W. Zhu, P. W. Kang, J. D. M. Silva and J. R., "Mechanisms and models of cardiac sodium channel inactivation," *Channels,* vol. 11, no. 6, pp. 517-533, 2017.

[23] A. Bazzone, A. J. Zabadne, A. Salisowski, M. G. Madej and K. Fendler, "A Loose Relationship: Incomplete H+/Sugar Coupling in the MFS Sugar Transporter GlcP," *Biophysical Journal,* vol. 113, no. 12, pp. 2736-2749, 2017.

[24] R. K. Henderson, K. Fendler and B. Poolman, "Coupling efficiency of secondary active transporters," *Current Opinion in Biotechnology,* vol. 58, pp. 62-71, 2019.

[25] C. Kettner, A. Bertl, G. Obermeyer, C. Slayman and H. Bihler, "Electrophysiological Analysis of the Yeast V-Type Proton Pump: Variable Coupling Ratio and Proton Shunt," *Biophys J.,* vol. 85, no. 6, p. 3730–3738, 2003.

[26] A. E. Robinson, N. E. Thomas, E. A. Morrison, B. M. Balthazor and a. K. A. Henzler-Wildman, "New free-exchange model of EmrE transport," *PNAS,* vol. 117, no. 47, pp. E10083-E10091, 2017.

[27] L. Shi, M. Quick, Y. Zhao, H. Weinstein and Jonathan A. Javitch, "The Mechanism of a Neurotransmitter:Sodium Symporter—Inward Release of Na+ and Substrate Is Triggered by Substrate in a Second Binding Site,," *Molecular Cell,* vol. 30, no. 6, pp. 667-677, 2008.

[28] A. Deckard and H. M. and Sauro, "Preliminary Studies on the In Silico Evolution of Biochemical Networks.," *ChemBioChem,* vol. 5, pp. 1423-1431, 2004.

[29] V. Menon, N. Spruston and W. L. Kath, "A state-mutating genetic algorithm to design ion-channel models," *PNAS,* vol. 106, no. 39, pp. 16829-16834, 2009.

[30] W. Gottstein, S. Müller, H. Herzel and R. Steuer, "Elucidating the adaptation and temporal coordination of metabolic pathways using in-silico evolution," *Biosystems,* vol. 117, pp. 68-76, 2014.

[31] Z. R. Teed and Jonathan R. Silva, "A computationally efficient algorithm for fitting ion channel parameters," *MethodsX,* vol. 3, pp. 577-588, 2016.

[32] S. A. Arrhenius, "Über die Dissociationswärme und den Einfluß der Temperatur auf den Dissociationsgrad der Elektrolyte," *Z. Phys. Chem.,* vol. 4, pp. 96-116, 1889.

[33] N. Metropolis, A. W. Rosenbluth, M. N. Rosenbluth and a. A. H. Teller, "Equation of State Calculations by Fast Computing Machines," *J. Chem. Phys.,* vol. 21, p. 1087, 1953.

[34] W. K. Hastings, "Monte Carlo sampling methods using Markov chains and their applications," *Biometrika,* vol. 57, no. 1, pp. 97-109, 1970.

[35] R. Phillips, J. Kondev, J. Theriot, H. Garcia, R. Phillips, J. Kondev, J. Theriot and H. Garcia, Physical Biology of the Cell, Garland Science, 2012.

[36] S. Whitelam and and Phillip L. Geissler, "Avoiding unphysical kinetic traps in Monte Carlo simulations of strongly attractive particles," *J. Chem. Phys.,* vol. 127, p. 154101, 2007.

[37] L. Rokach and O. Maimon, "Clustering Methods," in *Data Mining and Knowledge Discovery Handbook*, Springer, 2005, pp. 321-352.

[38] D. M. Zuckerman, "Physical Lens on the Cell," [Online]. Available: http://physicallensonthecell.org/cell-biology-phenomena/active-kinetic-proofreading. [Accessed 26 June 2019].

[39] M. D. McKay, R. J. Beckman and a. W. J. Conover, "A Comparison of Three Methods for Selecting Values of Input Variables in the Analysis of Output from a Computer Code," *Technometrics,* vol. 21, no. 2, pp. 239-245, 1979.